Cortical magnification underlies differences across but not around the visual field

Michael Jigo[1], Daniel Tavdy[1], & Marisa Carrasco[1,2]

[1]Center for Neural Science and [2]Department of Psychology,

New York University, New York, NY 1003

Keywords: contrast sensitivity, acuity, cortical magnification, performance fields, eccentricity, polar angle, visual field, M-scaling

Acknowledgments:

This work was supported by National Institutes of Health R01-EY027401 to M.C. We thank Antoine Barbot, Antonio Fernández, Nina Hanning, Marc Himmelberg, Shutian Xue and other members of the Carrasco lab, as well as Michael Landy for their helpful comments and discussion.

Author contributions

Conceptualization: M.J. and M.C. Methodology: M.J., D.T., and M.C. Investigation: M.J., D.T., and M.C. Visualization: M.J. Funding acquisition: M.C. Project administration: M.C. Supervision: M.C. Writing—original draft: M.J. and M.C. Writing—revision: M.J., D.T., and M.C.

Competing interests

The authors declare no competing interests.

Corresponding author:

Marisa Carrasco
Department of Psychology
New York University
6 Washington Place, Room 971
New York, NY 10003
Email: marisa.carrasco@nyu.edu

ABSTRACT

Performance changes dramatically both across (eccentricity) and around (polar angle) the visual field. All neurophysiological and virtually all behavioral studies of cortical magnification investigate eccentricity effects without considering polar angle. But, does cortical magnification underlie differences *around* the visual field? We magnified stimulus size according to eccentricity and polar angle to equate their cortical representation. We found that magnifying the stimulus eliminates differences across –but not around– the visual field.

MAIN

Contrast sensitivity, a fundamental visual capability, declines across eccentricity[1] and varies with polar angle: sensitivity is higher along the horizontal than vertical meridian –Horizontal-Vertical Anisotropy (HVA)– and along the lower than upper vertical meridian –Vertical Meridian Asymmetry (VMA)[2-7]. Cortical magnification, the linear extent of cortex corresponding to one degree of visual angle (mm/°), declines with eccentricity[8] and links behavior to brain structure[9-12] ('Quantitative' hypothesis). We magnified stimulus size according to striate-cortical neural density to equate the cortical area for stimuli at different visual field locations[13]. This M-scaling procedure eliminates the eccentricity effect on performance for many tasks[14] (e.g., contrast sensitivity and acuity; **Figure 1A**). Here, we assessed whether cortical magnification underlies polar angle asymmetries in contrast sensitivity (**Figure 1B**).

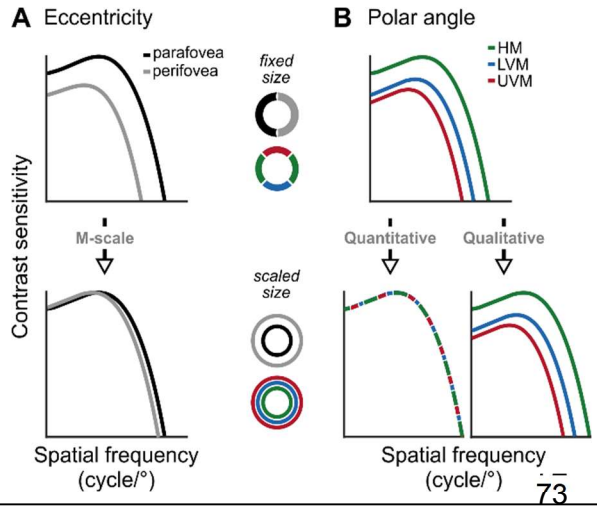

Figure 1. Schematic predictions of contrast sensitivity functions (CSFs). (**A**) CSFs decline between the parafovea (2°) and perifovea (6°) for fixed-sized gratings (top row), but differences at low and medium SFs diminish after M-scaling[13] (bottom row). (**B**) CSFs differ among the horizontal meridian (HM), lower vertical meridian (LVM) and upper vertical meridian (UVM) for fixed-sized stimuli (top row). If polar angle asymmetries derive from differences in neural density among locations, M-scaling will diminish them ('Quantitative' hypothesis). Alternatively, if the asymmetries derive from qualitatively different neural image-processing capabilities among locations, then M-scaling will not eliminate them ('Qualitative' hypothesis).

The contrast sensitivity function (CSF) characterizes stimulus visibility[1]. We measured human CSFs within the parafovea (2°) and perifovea (6°) at three polar angles: the horizontal meridian (HM), lower vertical meridian (LVM) and upper vertical meridian (UVM). While maintaining fixation, observers reported the orientation of a target grating for which contrast and spatial frequency (SF) varied on each trial (**Figure 2A**). We magnified perifoveal gratings following anisotropic M-scaling[13] to equate their cortical representation with parafoveal gratings (HM: 7.08°; LVM: 7.68°; UVM: 7.70°) and compare how CSFs changed after M-scaling.

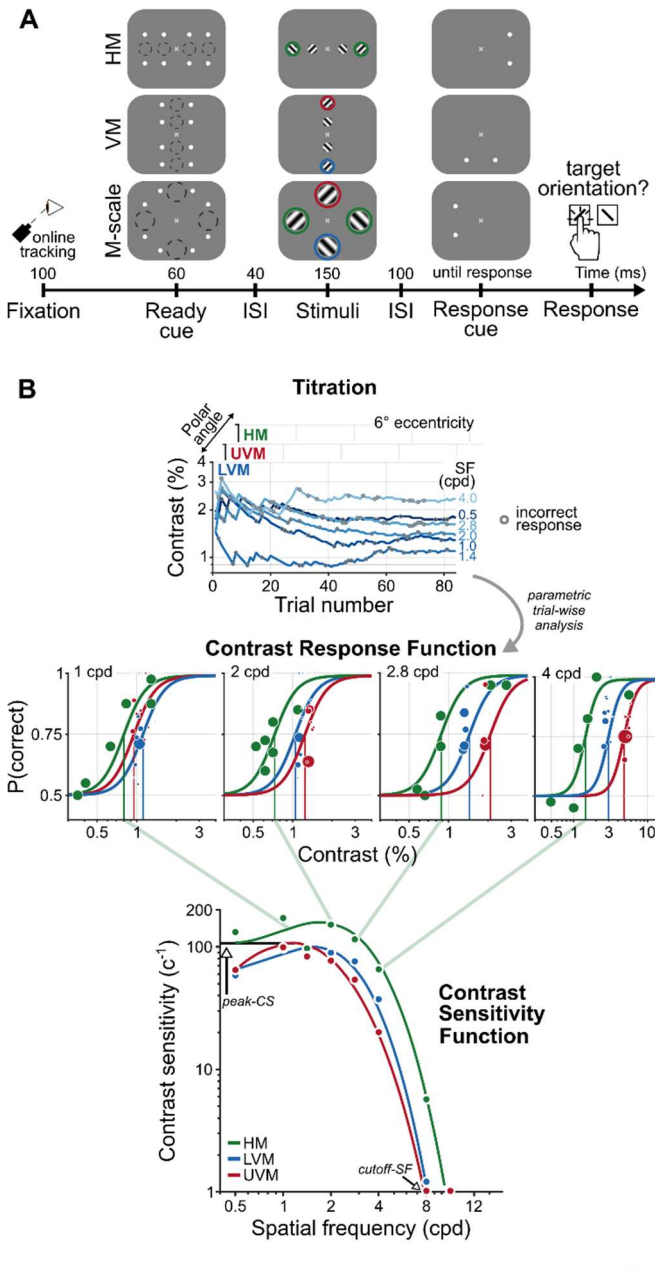

Figure 2. A psychophysical procedure to measure and a parametric model to characterize CSFs. (**A**) An example trial sequence for the orientation discrimination task. Each trial began with a fixation period, after which a cue indicated the onset of four gratings. The dashed circles illustrate the location and size of the grating stimuli; they did not appear during the experiment. Gratings appeared in the parafovea and perifovea, separately along the horizontal (HM) or vertical meridian (VM) or were M-scaled and presented simultaneously at each meridional location in the perifovea (M-scale). A response cue indicated which grating observers should report. By withholding the target location until response cue onset, we encouraged observers to maintain fixation throughout the trial. The colored circles indicate the perifoveal locations we compared to assess the impact of M-scaling on polar angle asymmetries: Green - HM, Blue - LVM, Red - UVM. (**B**) Parametric contrast sensitivity model. Grating contrast varied throughout the experiment following independent titration procedures for each eccentricity and polar angle location. Gray circles indicate incorrect responses for a given trial. A model composed of Contrast Response Functions (CRF) and CSFs constrained the relation between trial-wise performance, SF, eccentricity and polar angle. The diagonal green lines depict the connection between contrast thresholds from individual CRFs to contrast sensitivity on the CSF for the HM; contrast sensitivity is the inverse of contrast threshold. The colored dots in each CRF and CSF depict a representative observer's task performance and contrast sensitivity, determined directly from the titration procedures. The colored lines depict the best-fitting model estimates. We derived key attributes of the CSF – peak contrast sensitivity (peak-CS) and the acuity limit (cutoff-SF) –from the fitted parametric model.

We characterized observers' CSFs for the HM, VM and after M-scaling (**Figure 2A**) using a parametric contrast sensitivity model (**Figure 2B**, see *Online Methods*). We used model comparisons among nine CSF functional forms[15-17] to assess differences across eccentricity and polar angle for fixed-size gratings (**Supplementary Figure 1**). We extracted key CSF attributes–the peak contrast sensitivity (peak-CS) and acuity limit (cutoff-SF)–to characterize how contrast sensitivity changes with eccentricity, polar angle and M-scaling.

Contrast sensitivity peaked at a given SF and declined more rapidly for higher than lower SFs. We averaged CSFs across polar angle to isolate the eccentricity effect at 2°, 6° and after M-scaling perifoveal CSFs ($6°_{M\text{-}scale}$; **Figure 3A**). CSFs fell with eccentricity but less so after M-scaling. The eccentricity effect for fixed-size gratings, quantified as the percent change in contrast sensitivity for 2°, 6° and $6°_{M\text{-}scale}$, grew from ~30% to 120% across SF (**Figure 3B**).

After M-scaling, the eccentricity effect became negative for SFs <2 cpd: higher contrast sensitivity at $6°_{M\text{-}scale}$ than 2° (**Figure 3B**). A repeated-measures ANOVA (SF: 0.5-11cpd; stimulus size: fixed vs M-scaled) showed that M-scaling diminished the eccentricity effect differentially across SF (*interaction:* $F(7,63)=61.13$, $p<0.001$, $\eta_G^2=0.872$). Post hoc t-tests revealed significant reductions for all ($p<0.01$) but the two highest SFs (**Supplementary Table 1**), which reached the acuity limit. Thus, consistent with[9,14,18], M-scaling slightly reversed typical eccentricity effects for low SFs and reduced them for medium SFs (**Supplementary Figure 2**).

The HVA was pronounced at 2°, 6° and $6°_{M\text{-}scale}$ (**Figure 3C**). We quantified the HVA extent as the percent change in contrast sensitivity between the HM and VM (averaged LVM and UVM); positive values indicate higher sensitivity for the HM than VM. At 2° and 6°, the HVA extent increased from 20% to 120% across SF. Remarkably, this extent matched the eccentricity effect at high SFs. Thus, contrast sensitivity differences between the HM and VM at a fixed eccentricity were as pronounced as tripling stimulus eccentricity from 2° to 6°.

The HVA remained after M-scaling (**Figure 3D**). A two-way ANOVA compared its extent at the perifovea before and after M-scaling. Stimulus M-scaling reduced the HVA extent as a function of SF (*interaction:* $F(7,63)=7.32$, $p=0.0035$, $\eta_G^2=0.449$). For all but one SF (8 cpd: $p=0.021$, 95% CI=[1.26 57.37], $d=0.75$), M-scaling did not affect the HVA ($p>.05$). This finding supports the 'Qualitative' hypothesis–polar angle asymmetries do not derive from differences in the number

of neurons stimulated at each location but instead emerge from qualitatively different image-processing capabilities across polar angle (**Figure 1B**).

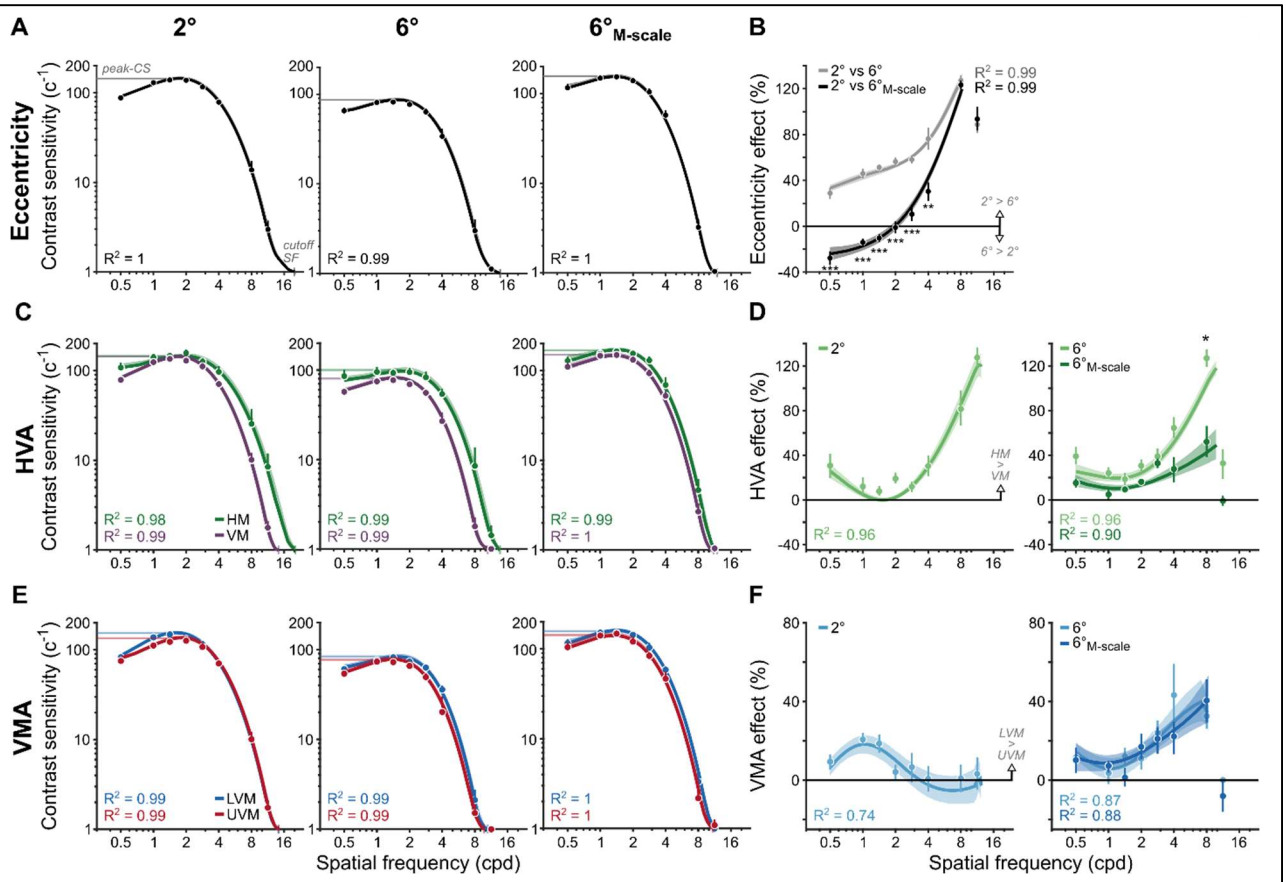

Figure 3. M-scaling diminishes the eccentricity effect, but neither the HVA nor the VMA. (**A**) CSFs averaged across polar angles for fixed-size gratings at 2° and 6°, as well as for M-scaled gratings at 6°. (**B**) Eccentricity effects are quantified as the percent change in contrast sensitivity between 2°and 6° as well as between 2° and 6°$_{M\text{-}scale}$. Positive values indicate higher contrast sensitivity at 2° than 6°. Negative values indicate a reversal: higher contrast sensitivity at 6° than 2°. (**C**) CSFs for the HM compared to the average CSF across the LVM and UVM. (**D**) The percent change between horizontal and vertical meridians at 2° (left) and the percentage change between meridians for 6° and 6°$_{M\text{-}scale}$ (right). Values above 0% indicate higher sensitivity for the HM than VM. (**E**) CSFs for the LVM and UVM. (**F**) The percent change between LVM and UVM following the conventions in D (with a truncated y-axis); positive values indicate higher sensitivity for the LVM than UVM. All dots correspond to the group-average contrast sensitivity and percent change in contrast sensitivity, as estimated from the titration procedures. All lines correspond to the group-average fit of the parametric contrast sensitivity model. Error bars and shaded areas denote bootstrapped 68% confidence intervals. *p<0.05, **p<0.01, ***p<0.001.

The VMA emerged at 2°, 6° and 6°$_{M\text{-}scale}$ (**Figure 3E**). We quantified the VMA extent as the percent change in contrast sensitivity between the LVM and UVM (**Figure 3F**). For fixed-size and M-scaled gratings, the VMA extent reached a maximum of 40% at 1 cpd in the parafovea

and 8 cpd in the perifovea. The VMA had only been characterized at eccentricities >2°[2-4,6,7]. This near-foveal location reveals that the SF at which the VMA peaks depends on eccentricity.

M-scaling did not affect the VMA (**Figure 3F**). A two-way ANOVA found a main effect of SF ($F(7,63)=10.16$, $p<0.001$, $\eta_G^2=0.53$) due to an increasing perifoveal VMA extent across SF. We found neither a main effect of stimulus size nor an interaction effect ($p>0.1$), indicating no difference in VMA extent before and after M-scaling. This finding further supports the 'Qualitative' hypothesis for polar angle asymmetries.

Key CSF attributes–peak-CS and cutoff-SF–displayed changes consonant with eccentricity effects and polar angle asymmetries (**Figure 4**), but peak-SF and SF-bandwidth did not (**Supplementary Figure 3**). We assessed each attribute with separate repeated-measures ANOVAs for the HVA and VMA across eccentricity and polar angle.

The HVA emerged in the peak-CS only in the perifovea (*interaction:* $F(2,18)=18.33$, $p<0.001$, $\eta_G^2=0.671$; **Figure 4A**). Peak-CS fell between 2° and 6° (*HVA*: $p<0.001$, 95% CI=[0.404 0.555], $d=4.52$; *VMA*: $p<0.001$, 95% CI=[0.513 0.651], $d=6.039$), increased in the perifovea after M-scaling (*HVA*: $p<0.001$, 95% CI=[-0.639 -0.483], $d=-5.14$; *VMA*: $p<0.001$, 95% CI=[-0.681 -0.562], $d=-7.50$) and did not differ between 2° and $6°_{\text{M-scale}}$ ($p>0.1$). Importantly, differences between HM and VM only emerged at 6° ($p<0.001$, 95% CI=[0.153 0.318], $d=2.04$) and $6°_{\text{M-scale}}$ ($p<0.01$, 95% CI=[0.054 0.175], $d=1.35$). In contrast, the VMA emerged at 2°, 6° and $6°_{\text{M-scale}}$ (*polar angle main effect*: $F(1,9)=8.65$, $p<0.02$, $\eta_G^2=0.490$; **Figure 4B**). These findings show that the HVA and VMA emerged in peak-CS, but the HVA only in the perifovea whereas the VMA at both eccentricities. Moreover, although M-scaling matched the peak-CS between the parafovea and perifovea, it did not equate contrast sensitivity around polar angle.

The HVA and VMA also emerged in the cutoff-SF, consistent with[19,20]. M-scaling reduced the HVA extent (*interaction:* $F(2,18)=19.20$, $p<0.001$, $\eta_G^2=0.681$; **Figure 4C**). The cutoff-SF decreased between HM and VM at 2° ($p<0.001$, 95% CI=[0.227 0.403], $d=2.56$), 6° ($p<0.001$, 95% CI=[0.231 0.324], $d=4.24$) and slightly less so at $6°_{\text{M-scale}}$ ($p=0.0326$, 95% CI=[0.0251 0.146], $d=1.01$). Thus, M-scaling did not eliminate either the HVA or the eccentricity effect in the cutoff-SF; it was smaller at 6° ($p<0.001$, 95% CI=[0.318 0.409], $d=5.73$) and $6°_{\text{M-scale}}$ ($p<0.001$, 95% CI=[0.324 0.431], $d=5.07$) than at 2°.

The VMA extent in cutoff-SF only emerged in the perifovea (*interaction:* F(2,18)=5.26, p=0.029, η_G^2=0.369; **Figure 4D**). It decreased between the LVM and UVM at 6° (p=0.0397, 95% CI=[0.0185 0.121], d=0.972) and 6°$_{M\text{-}scale}$ (p=0.0481, 95% CI=[0.0163 0.123], d=0.935). Therefore, M-scaling did not eliminate either the VMA or the eccentricity effect in cutoff-SF (*2°>6°*: p<0.001, 95% CI=[0.297 0.391], d=5.25; *2°>6°$_{M\text{-}scale}$*: p<0.001, 95% CI=[0.235 0.291], d=6.73). But it increased the perifoveal cutoff-SF along the vertical meridian (*6°$_{M\text{-}scale}$>6°*: p<0.005, 95% CI=[-0.119 -0.0437], d=-1.54). In short, the HVA in cutoff-SF occurred at both eccentricities but only in the perifovea for the VMA. Critically, M-scaling did not equate cutoff-SF among polar angles.

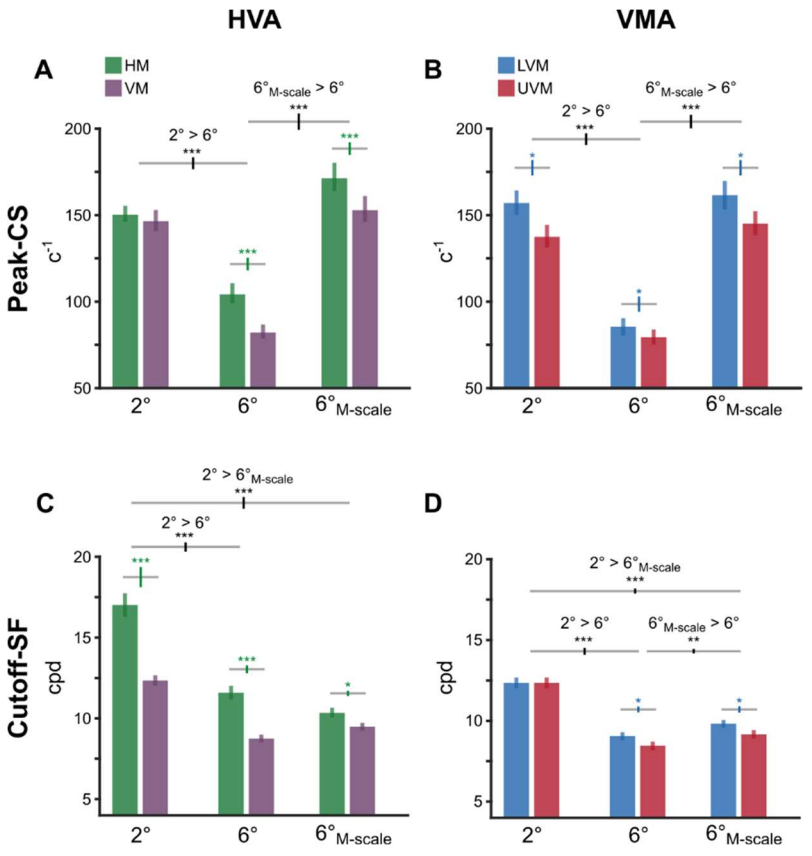

Figure 4. Polar angle asymmetries emerge in key CSF attributes. (**A-B**) Peak contrast sensitivity for the HVA and VMA, respectively. (**C-D**) Cutoff-SF for the HVA and VMA, respectively. Each bar depicts the group-average attribute at a given location and error bars depict bootstrapped 68% confidence intervals. Horizontal gray lines denote significant comparisons of an ANOVA and of post hoc comparisons. The vertical lines displayed on the gray bars depict the 68% confidence interval for the differences between eccentricities or locations. *p<0.05, **p<0.01, ***p<0.001.

Converging neural evidence demonstrates that cortical magnification limits peripheral vision. The striate-cortical surface area across eccentricity correlates with various perceptual measures, including acuity[10,12], perceived angular size[21] and perceived object size[11]. These perceptual differences across eccentricity derive from quantitative differences in the number of neurons for foveal and peripheral eccentricities. Consequently, accounting for cortical magnification via M-scaling diminishes eccentricity effects but not polar angle asymmetries.

Optical and retinal factors only partially explain higher sensitivity for the HM than VM (<20%) and even less for the LVM than UVM (<5%)[22]. Psychophysical measures of acuity[20,23] and contrast sensitivity[6,7] correlate with the >60% more striatal surface area for the HM than VM and >25% for the LVM than UVM[7,23]. However, compensating for striate-cortical magnification around the visual field did not equate contrast sensitivity. These findings further support the 'Qualitative' hypothesis (**Figure 1B**).

M-scaling did not nullify polar angle asymmetries either across the CSF or its peak-CS and cutoff-SF. The apparent reduction in the HVA extent at a high SF (8 cpd, **Figure 3D**) may have resulted from the low cutoff-SF in the perifoveal VM. The perifoveal cutoff-SF remained at 8 cpd (**Figure 4C**) and yielded a noisier measure of the HVA extent. Nonetheless, M-scaling greatly diminished the eccentricity effect while preserving the HVA and the VMA at low and medium SFs.

Using psychophysics to probe the neural substrates of perceptual asymmetries, we show that structural constraints of cortical magnification do not underlie polar angle asymmetries. By revealing that cortical magnification limits perception across eccentricity–but not around polar angle—these findings challenge the M-scaling account of visual perception[9-14].

In conclusion, we show that striking differences around polar angle, which are as pronounced as tripling eccentricity, remain after M-scaling. These findings challenge the established view that cortical magnification limits basic visual perception throughout the visual field[9-14]. Models of spatial vision linking brain and behavior should account for what constrains basic visual perception not only across –but also around– the visual field.

ONLINE METHODS

Observers

We based our sample size on research on the impact of eccentricity[24] and visual performance fields on contrast sensitivity[6] and acuity[20]. Ten observers with normal or corrected-to-normal vision participated in three conditions (8 female, aged 21 - 32 years, two authors: M.J and D.T). All observers provided written informed consent under the University Committee's protocol on Activities Involving Human Subjects at New York University. All experimental procedures were in agreement with the Declaration of Helsinki. All observers, except the authors, were naïve to the purpose of the study and were paid $12/hour.

Stimuli

Gratings. Sinusoidal gratings with a SF of 0.5, 1, 1.4, 2, 2.8, 4, 8, or 11.3 cycles per degree (cpd) served as targets. For the HM condition, stimuli appeared along the left and right horizontal meridian at 2° and 6° eccentricity. Similarly, stimuli appeared at the same eccentricities but along the upper and lower vertical meridian for the VM condition. During the HM and VM conditions, a two-dimensional cosine function (4° wide, centered on the grating's peak luminance) windowed each grating. For the M-scale condition, gratings appeared at 6° eccentricity along horizontal and vertical meridians. We scaled their sizes separately for each polar angle resulting in gratings that subtended 7.68° for the LVM, 7.70° for the UVM and 7.08° for the HM following the equations in[13].

Specifically, we computed M-scaled sizes as:

$$S_{X_b} = \frac{S_{X_a} \times M_{X_a}}{M_{X_b}} \quad (1)$$

where S_{X_b} corresponds to the magnified size in degrees of visual angle along meridian X at eccentricity b. This M-scaled size equates the cortical representation with that of a grating of size S_{X_a}, which equaled 4°, positioned along the same meridian but at a different eccentricity a. M_{X_a} and M_{X_b} correspond to cortical magnification in mm/° along a given meridian X at eccentricity a and b respectively.

Cortical magnification differed among meridians. For the LVM:

$$M_{LVM} = M_0(1 + 0.42E + 0.000055E^3)^{-1} \quad (2)$$

where M_0 corresponds to cortical magnification at the central fovea, which was set to 7.99 mm/° and E corresponds to the eccentricity of the stimulus.

Similarly, for the UVM:

$$M_{UVM} = M_0(1 + 0.42E + 0.00012E^3)^{-1} \quad (3)$$

For the HM, we used the cortical magnification equations for both the Nasal (N) and Temporal (T) meridians:

$$M_N = M_0(1 + 0.33E + 0.00007E^3)^{-1} \quad (4)$$

$$M_T = M_0(1 + 0.29E + 0.000012E^3)^{-1} \quad (5)$$

and computed the M-scaled size at eccentricity b for the HM (S_{HM_b}) using the average among M-scaled sizes for Nasal (S_{N_b}) and Temporal meridians (S_{T_b}):

$$S_{HM_b} = 0.5(S_{N_b} + S_{T_b}) \quad (6)$$

Cues. 'Ready cues' prepared observers for the onset of the grating stimuli and 'response cues' indicated which grating to report. Response cues comprised a pair of white dots (56 cd/m^2) displaced 3.75° from the vertical or horizontal meridian for target gratings that appeared at those respective locations. Ready cues comprised the same white dots that appeared at all possible target locations for the HM and VM conditions.

Fixation and background. Observers maintained their gaze on a dim, gray fixation cross (17 cd/m^2) that subtended 0.35° throughout each trial. All stimuli appeared on a medium gray background (26 cd/m^2).

Apparatus

We generated visual stimuli on an Apple iMac using MGL[25], a set of OpenGL libraries running in MATLAB (MathWorks, Natick, MA, USA) and displayed them on a cathode ray tube (CRT) monitor (1280 x 960; 100 Hz). We gamma-corrected the monitor using a Konica Minolta LS-100 (Tokyo, Japan). Observers sat in a dark and quiet room and viewed the display binocularly with their heads stabilized by a chin-and-head rest positioned either 57 cm (VM and M-scale conditions) or 115 cm (HM condition, to display the highest SF tested, 16 cpd). An Eyelink 1000 eye tracker (S.R. Research, Ottawa, Ontario, Canada) monitored monocular eye position at 500 Hz.

345

346 **Behavioral protocol**

347 We instructed observers to maintain fixation. Stimulus presentation was contingent upon fixation
348 on a central cross for 100 ms, after which the ready cue appeared (60 ms for the dots, 300 ms
349 for the 'N'). The cue informed observers of the temporal onset of the target grating but provided
350 no information about its location. Following an interstimulus interval (ISI; 40 ms for the dots, 100
351 ms for the 'N'), four gratings with the same SF appeared for 150 ms. Grating contrast varied in
352 individual trials, determined by independent adaptive titration procedures for each grating (see
353 *Titration*). A 100-ms ISI and the response cue followed the grating presentation. The response
354 cue indicated which grating observers should report on each trial. Observers performed an
355 orientation discrimination task. They used the right or left arrow keys on a keyboard to report
356 whether the cued grating tilted to the right or left of vertical. If the eye blinked or deviated >1°
357 from fixation, the trial was immediately aborted and rerun at the end of the block.

358

359 We instructed observers to be as accurate as possible without time stress. They received
360 auditory feedback for incorrect responses on a trial-by-trial basis. Once observers finished a
361 block, the monitor displayed their overall accuracy (percent correct) as feedback.

362

363 **Procedure**

364 Observers performed three conditions: HM, VM and M-scale. For the HM condition, they
365 completed 1080 trials per location, for the VM condition 1344 per location and for the M-scale
366 condition 1008 per location. On each trial, we randomly interleaved the target's orientation, SF,
367 eccentricity and/or polar angle, and adjusted grating contrast based on task performance (see
368 *Titration*). Before the main experimental sessions, observers completed a single block of trials to
369 familiarize themselves with the stimuli and task.

370

371 **Titration**

372 For VM and M-scale conditions, we titrated contrast separately for each combination of SF,
373 eccentricity and polar angle with best PEST, a maximum likelihood adaptive procedure, using
374 custom code (https://github.com/michaeljigo/palamedes_wrapper) that ran subroutines
375 implemented in the Palamedes toolbox[26]. For HM, we used a 3-down, 1-up weighted
376 staircase[24]. Both titration procedures targeted 75% task performance.

377

378

Parametric contrast sensitivity model

We fit a parametric model that linked contrast response functions (CRFs) and contrast sensitivity functions (CSFs) to observers' binary decisions (CW vs CCW) on individual trials. Our model includes 1) a logistic function for the CRF, with slope fixed across SF[24] and asymptotes matched to the specifications of the adaptive titration procedure; 2) nine candidate models of the CSF; 3) six visual field models that specify how contrast sensitivity changes with eccentricity and polar angle.

CRF. We characterized the CRF –performance as a function of $\log_{10}$-transformed contrast— using a logistic function (Equation 7) with lower and upper asymptotes ($p_l = 0.5$, $p_u = 0.99$) and slope ($\kappa = 11.8$) matching the specifications of the adaptive titration procedure, as well as a $\log_{10}$-transformed contrast threshold ($c_t(f, r, \theta)$, Equation 8) that targets 75% discrimination accuracy (p_t=0.75) at each SF (f), eccentricity (r) and polar angle (θ):

$$p(c, f, r, \theta) = s\left(\frac{1}{1 + \exp(-\kappa(c - t))}\right) + p_l \tag{7}$$

where $s = 1 - (1 - p_u) - p_l$, which scales the dynamic range of the function. Because contrast was $\log_{10}$-transformed, adjusting the contrast threshold in Equation 7 yields rigid shifts in logarithmic contrast.

In equation 7, t corresponds to a transformation of contrast threshold, which ensures p_t is accurately targeted given the constraints of the logistic function's slope, upper and lower asymptotes:

$$t(c_t(f, r, \theta), p_r) = c_t(f, r, \theta) - \kappa^{-1} \log\left(\frac{p_r}{1 - p_r}\right) \tag{8}$$

where p_r denotes the ratio between the targeted performance level and the dynamic range of the CRF: $p_r = \frac{p_t - p_l}{s}$.

CSF. Contrast sensitivity typically peaks at a given SF and declines precipitously for higher SFs and gradually for lower SFs[15-17]. We implemented this pattern by constraining the contrast threshold ($c_t(f, r, \theta)$ in Equation 8) across SF to adhere to a functional form of the CSF. We

implemented nine candidate CSF models that each determined contrast sensitivity (c_t^{-1}) as a function of SF (f) at each eccentricity (r) and polar angle (θ) using 3 or 4 parameters (**Table 1**).

Table 1. Candidate CSF models. The number of parameters included in each model (*n*) is denoted under the corresponding label, along with a brief description and the model equation. The bolded entry indicates the best-fitting model.

Label *(n)*	Description	Equation
YQM *(4)*	**Derived from a model of contrast sensitivity[16]**	$c_t^{-1}(f,r,\theta;\alpha,\beta,\gamma,\delta) = \delta[\frac{\exp(-f/\alpha)}{1+\frac{\gamma}{1+(f/\beta)}}]$
dEXP *(3)*	Double exponential function[15]	$c_t^{-1}(f,r,\theta;\alpha,\beta,\delta) = \delta f^{\alpha}\exp(-f/\beta)$
aLP *(4)*	Asymmetric log parabola[17]	$c_t^{-1}(f,r,\theta;\alpha,\beta,\gamma,\delta)=\begin{cases}\delta-(f-\alpha)^2\beta^2 & \text{if f}<\alpha\\ \delta-(f-\alpha)^2\gamma^2 & \text{if f}\geq\alpha\end{cases}$
DoG *(4)*	Difference of Gaussians[16]	$c_t^{-1}(f,r,\theta;\alpha,\beta,\gamma,\delta) = \delta(\exp[-(f/\alpha)^2]-\gamma\exp[-(f/\beta)^2])$
LP *(3)*	Log parabola[16]	$c_t^{-1}(f,r,\theta;\alpha,\beta,\delta) = \delta\exp[-(\frac{\log_2(f/\alpha)}{\beta})^2]$
MS *(4)*	Generalized Gaussian with linear function of SF[16]	$c_t^{-1}(f,r,\theta;\alpha,\beta,\gamma,\delta) = \delta(1-\beta+\frac{f}{\alpha})\exp[-(f/\alpha)^{\gamma}]$
HmH *(4)*	Difference of hyperbolic secants[16]	$c_t^{-1}(f,r,\theta;\alpha,\beta,\gamma,\delta) = \delta(\text{sech}[f/\alpha]-\gamma\text{sech}[f/\beta])$
HmG *(4)*	Hyperbolic secant minus a Gaussian[16]	$c_t^{-1}(f,r,\theta;\alpha,\beta,\gamma,\delta) = \delta(\text{sech}[f/\alpha]-\gamma\exp[-(f/\beta)^2])$
EmG *(4)*	Exponential minus a Gaussian[16]	$c_t^{-1}(f,r,\theta;\alpha,\beta,\gamma,\delta) = \delta(\exp[-f/\alpha]-\gamma\exp[-(f/\beta)^2])$

Visual field models. We implemented six models specifying how CSFs change across eccentricity and polar angle. For each model, we iteratively fixed the CSF's parameters to permit or restrict the impact of eccentricity, HVA and/or VMA on contrast sensitivity (**Supplementary Figure 1**). For example, the most permissive model ("Ecc + HVA + VMA", **Table 2**) allowed CSFs to vary freely across eccentricity and polar angle, which yielded 24 parameters for CSF models with four parameters (e.g., YQM model, **Table 1**; 4 parameters x 2

eccentricities x 3 polar angles = 24 parameters, **Table 2**). In contrast, the most restrictive model ("-Ecc - HVA - VMA", **Table 2**) enforced a single CSF at all visual field locations, yielding only four parameters. A detailed breakdown of the model alternatives is presented in **Table 2**. We additionally assessed whether CSFs depended on the pre-cue presented to observers in the fixed-size conditions and found that they did not.

Table 2. Models of contrast sensitivity across eccentricity and polar angle. The bolded entry indicates the best-fitting model.

Model label	Description	Max number of parameters
Ecc + HVA + VMA	**CSFs vary across eccentricity and polar angle**	**24**
Ecc + HVA - VMA	CSFs do not vary along the VM	16
Ecc - HVA + VMA	CSFs do not vary along the HM	16
-Ecc + HVA + VMA	CSFs do not vary across eccentricity	12
Ecc - HVA - VMA	CSFs do not vary along the VM and HM	8
-Ecc - HVA - VMA	CSFs are identical at all visual field locations	4

Model fitting. Our parametric contrast sensitivity model generates the probability that an observer will correctly judge a grating's orientation as a function of contrast, SF and visual field location (Equation 7). We optimized the model's parameters via maximum likelihood estimation. We considered an observer's task performance at each contrast, SF, eccentricity and polar angle as independent Bernoulli random variables and minimized the negative log-likelihood for an observer's responses using fmincon in the MATLAB Optimization Toolbox. This procedure maximized the power of our analyses by leveraging each data point (i.e., trial).

We performed model fitting in two stages to: 1) identify the best-fitting CSF model and 2) determine the appropriate visual field model. To identify the best CSF model, we fit each CSF model (**Table 1**) to each observer's behavioral responses across all three conditions (HM, VM and M-scale). For these fits, the CSFs followed the most permissive visual field model (Ecc + HVA + VMA, **Table 2**). Model comparisons determined the best-fitting CSF model (see *Model comparisons*).

After identifying the best CSF model, we determined which visual field model corresponded best to observers' contrast sensitivity across eccentricity and polar angle. To this end, we fit each visual field model (**Table 2**) to each observer's responses to fixed-size grating stimuli (HM and VM conditions) because these stimuli yield robust variations in contrast sensitivity across eccentricity and polar angle[1,6,9,18,24]. For these fits, we used the best-fitting CSF model identified in stage 1.

Model comparisons

We compared CSF models (**Table 1**) and visual field models (**Table 2**). The difference in BIC values between model variants indexed model performance, with lower values corresponding to better performance. We calculated BIC values as: $BIC = -2k\log(n)L$ where k denotes the number of model parameters, n denotes the number of trials, and L corresponds to a model's maximized log-likelihood.

Quantifying the extent of eccentricity effects and polar angle asymmetries

We quantified the impact of changing visual field location (e.g., 2° to 6°) as the percent change in contrast sensitivity (Δc_t^{-1}) between one location (l_1) and the other (l_2), normalized by the average contrast sensitivity among locations: $\Delta c_t^{-1} = 100\frac{l_1 - l_2}{0.5(l_1 + l_2)}$.

CSF attributes

We extracted key CSF attributes from the best-fitting model: peak-CS, peak-SF, cutoff-SF and SF bandwidth. Because not all CSF models in **Table 1** have parameters that map onto these attributes, we evaluated each observer's best-fitting CSF between 0.25 cpd and 24 cpd. We defined the peak-CS as the maximum contrast sensitivity of the CSF, the peak-SF as the SF at which peak-CS occurred, the cutoff-SF as the SF at which contrast sensitivity reached its minimum value of 1 and the SF bandwidth as the number of octaves spanned at the CSF's full-width-at-half-maximum.

Statistical analyses

We used repeated measures ANOVAs followed by paired t-tests for post hoc comparisons. All post hoc comparisons were Bonferroni-corrected for multiple comparisons. All p-values for repeated-measures ANOVAs in which the assumption of sphericity was not met were Greenhouse-Geisser corrected. Each ANOVA assessed how M-scaling affected the extent of

478 eccentricity effects and polar angle asymmetries. We used separate ANOVAs to assess how M-
479 scaling affected the perifoveal HVA and VMA. We report effect sizes in terms of generalized eta
480 squared (η_G^2) for ANOVAs and Cohen's d for t-tests.

REFERENCES

1. Robson, J.G. & Graham, N. Probability summation and regional variation in contrast sensitivity across the visual field. *Vision Research* **21**, 409-418 (1981).
2. Carrasco, M., Talgar, C.P. & Cameron, E.L. Characterizing visual performance fields: Effects of transient covert attention, spatial frequency, eccentricity, task and set size. *Spatial Vision* **15**, 61-75 (2001).
3. Cameron, E.L., Tai, J.C. & Carrasco, M. Covert attention affects the psychometric function of contrast sensitivity. *Vision Research* **42**, 949-967 (2002).
4. Abrams, J., Nizam, A. & Carrasco, M. Isoeccentric locations are not equivalent: The extent of the vertical meridian asymmetry. *Vision Research* **52**, 70-78 (2012).
5. Baldwin, A.S., Meese, T.S. & Baker, D.H. The attenuation surface for contrast sensitivity has the form of a witch's hat within the central visual field. *Journal of Vision* **12**, 23-23 (2012).
6. Himmelberg, M.M., Winawer, J. & Carrasco, M. Stimulus-dependent contrast sensitivity asymmetries around the visual field. *Journal of Vision* **20**, 18-18 (2020).
7. Himmelberg, M.M., Winawer, J. & Carrasco, M. Linking individual differences in human primary visual cortex to contrast sensitivity around the visual field. *bioRxiv*, 2021.2010.2004.463138 (2022).
8. Van Essen, D.C., Newsome, W.T. & Maunsell, J.H. The visual field representation in striate cortex of the macaque monkey: asymmetries, anisotropies, and individual variability. *Vision Research* **24**, 429-448 (1984).
9. Rovamo, J., Virsu, V. & Näsänen, R. Cortical magnification factor predicts the photopic contrast sensitivity of peripheral vision. *Nature* **271**, 54-56 (1978).
10. Duncan, R.O. & Boynton, G.M. Cortical magnification within human primary visual cortex correlates with acuity thresholds. *Neuron* **38**, 659-671 (2003).
11. Schwarzkopf, D.S., Song, C. & Rees, G. The surface area of human V1 predicts the subjective experience of object size. *Nature Neuroscience* **14**, 28-30 (2011).
12. Song, C., Schwarzkopf, D.S., Kanai, R. & Rees, G. Neural population tuning links visual cortical anatomy to human visual perception. *Neuron* **85**, 641-656 (2015).
13. Rovamo, J. & Virsu, V. An estimation and application of the human cortical magnification factor. *Experimental Brain Research* **37**, 495-510 (1979).
14. Strasburger, H., Rentschler, I. & Jüttner, M. Peripheral vision and pattern recognition: A review. *Journal of Vision* **11**, 13-13 (2011).
15. Movshon, J.A. & Kiorpes, L. Analysis of the development of spatial contrast sensitivity in monkey and human infants. *JOSA A* **5**, 2166-2172 (1988).
16. Watson, A.B. & Ahumada, A.J. A standard model for foveal detection of spatial contrast. *Journal of Vision* **5**, 6 (2005).
17. Chung, S.T.L. & Legge, G.E. Comparing the Shape of Contrast Sensitivity Functions for Normal and Low Vision. *Investigative Opthalmology & Visual Science* **57**, 198 (2016).
18. Virsu, V. & Rovamo, J. Visual resolution, contrast sensitivity, and the cortical magnification factor. *Experimental Brain Research* **37** (1979).
19. Wilkinson, M.O., Anderson, R.S., Bradley, A. & Thibos, L.N. Neural bandwidth of veridical perception across the visual field. *Journal of vision* **16**, 1-1 (2016).
20. Barbot, A., Xue, S. & Carrasco, M. Asymmetries in visual acuity around the visual field. *Journal of Vision* **21**, 2-2 (2021).
21. Murray, S.O., Boyaci, H. & Kersten, D. The representation of perceived angular size in human primary visual cortex. *Nature Neuroscience* **9**, 429-434 (2006).
22. Kupers, E.R., Benson, N.C., Carrasco, M. & Winawer, J. Asymmetries around the visual field: From retina to cortex to behavior. *PLOS Computational Biology* **18**, e1009771 (2022).

23. Benson, N.C., Kupers, E.R., Barbot, A., Carrasco, M. & Winawer, J. Cortical magnification in human visual cortex parallels task performance around the visual field. *Elife* **10**, e67685 (2021).
24. Jigo, M. & Carrasco, M. Differential impact of exogenous and endogenous attention on the contrast sensitivity function across eccentricity. *Journal of Vision* **20**, 11 (2020).
25. Gardner, J.L., Merriam, E.P., Schluppeck, D. & Larsson, J. MGL: Visual psychophysics stimuli and experimental design package. (Zenodo, 2018).
26. Prins, N. & Kingdom, F.A.A. Applying the Model-Comparison Approach to Test Specific Research Hypotheses in Psychophysical Research Using the Palamedes Toolbox. *Frontiers in Psychology* **9** (2018).

SUPPLEMENTARY MATERIALS

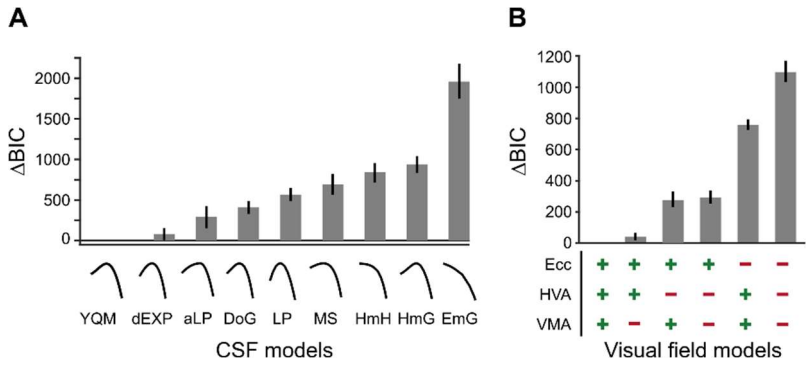

Supplementary Figure 1. BIC model comparisons for CSF and visual field models. (**A**) CSF model comparisons for the nine candidate functional forms of the CSF (**Table 1**). Low ΔBIC values indicate superior model performance. Curves under each bar illustrate the best fit of each CSF model to a representative observer. (**B**) Visual field model comparisons (**Table 2**). '+' and '-' under each bar indicate the components included and excluded, respectively, in each model. For example, '+' for 'HVA' indicates that CSFs could change between the horizontal and vertical meridians whereas a '-' indicates that CSFs for the horizontal meridian were identical to the lower vertical meridian.

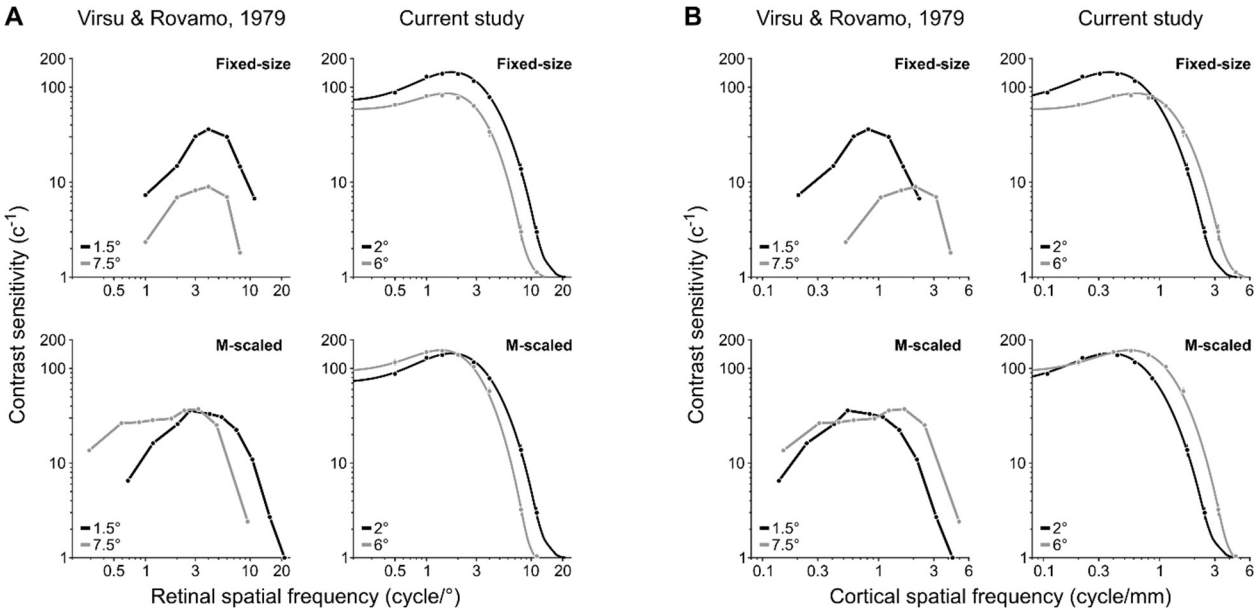

Supplementary Figure 2. Qualitatively similar CSFs between previous reports[18] and the current study for fixed-size and M-scaled grating stimuli. (**A**) CSFs expressed as a function of retinal SF. For fixed-size stimuli, CSFs decline with increasing eccentricity at all SFs. After M-scaling, contrast sensitivity for the farther eccentricity exceeds that of the nearer eccentricity at low SFs. (**B**) CSFs expressed as a function of cortical SF. We used equations in[18] to determine the SF when projected onto the cortical surface at each eccentricity, resulting in the cycles per millimeter of striate-cortical surface area. The data for 'Virsu & Rovamo, 1979' depict contrast sensitivity for an individual observer as plotted in Figure 4 of[18]. We extracted only the eccentricities most comparable to those tested in the current study. The CSFs displayed under 'Current study' follow the conventions of **Figure 3** in the main text.

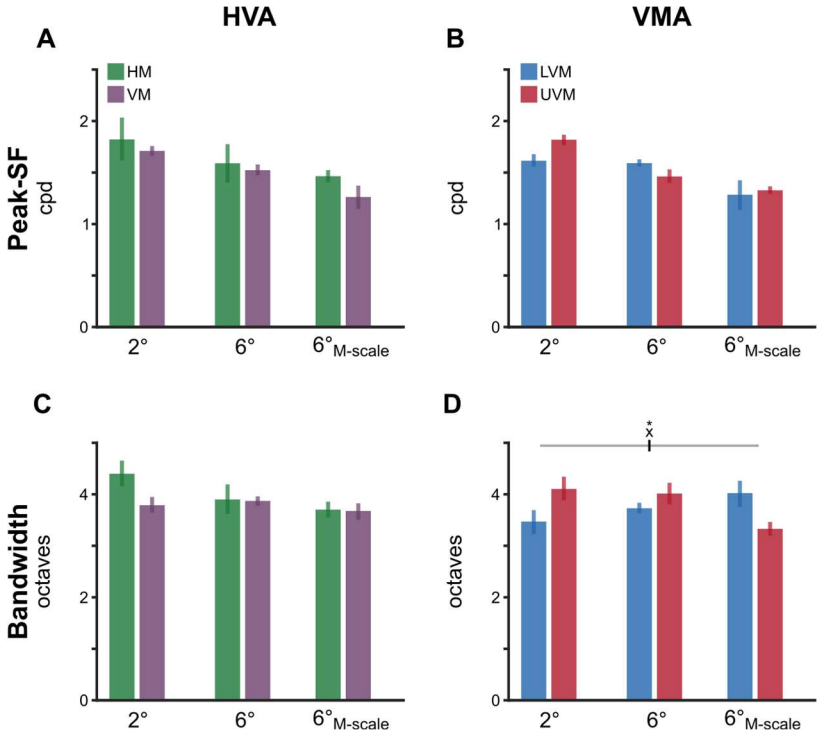

Supplementary Figure 3. Neither polar angle asymmetries nor eccentricity effects emerge in retinal peak SF and SF bandwidth. (**A-B**) Peak SF for the HVA and VMA, respectively. (**C-D**) SF bandwidth for the HVA and VMA, respectively. Each bar depicts the group-average attribute at a given meridional location and error bars depict 68% confidence intervals. A significant interaction emerged in the bandwidth for the VMA ($F(2,18)=5.21$, $p=0.019$, $\eta_G^2=0.367$). However, none of the post hoc comparisons reached significance (all $p>0.1$). No other statistical comparisons were significant.

571 **Supplementary Table 1.** Statistics for post hoc comparisons of eccentricity effect.

SF (cpd)	P-value	95% CI	Cohen's *d*
0.5	<0.001	[46.80 67.53]	3.95
1	<0.001	[54.55 67.32]	6.83
1.4	<0.001	[51.74 65.13]	6.25
2	<0.001	[43.46 60.92]	4.28
2.8	<0.001	[30.80 54.90]	2.54
4	<0.01	[16.60 47.25]	1.49
8	1	[-5.70 24.45]	0.45
11	>.1	[-13.91 -0.38]	0.76

572